Proceedings of the 2007 American Control Conference
Marriott Marquis Hotel at Times Square
New York City, USA, July 11-13, 2007

$\mathcal{L}_1$ Adaptive Control of a UAV for Aerobiological Sampling

Jiang Wang[1], Vijay Patel[1], Craig A. Woolsey[1], Naira Hovakimyan[1] & David Schmale, III[2]
[1]Department of Aerospace & Ocean Engineering
[2]Department of Plant Pathology, Physiology, and Weed Science
Virginia Polytechnic Institute and State University, Blacksburg, VA 24061
{jwang005,vvp2069,cwoolsey,nhovakim,dschmale}@vt.edu

***Abstract*— Small unmanned air vehicles (UAVs) have been used to collect samples of pollen, plant pathogens, and other biological particles within the earth's surface boundary layer (from about one to fifty meters altitude) and the planetary boundary layer (from about fifty to one thousand meters). These samples provide valuable information concerning the release, transport, and deposition of biological particles, with important implications for food safety and agricultural practices. In some sampling applications, it is essential that the UAV's speed and altitude be precisely regulated, which suggests the use of an autopilot. Because the biological sampling apparatus may dramatically alter the UAV's flying qualities, however, the autopilot must be robust to large, fast changes in the dynamic model parameters. This paper describes the application of a new adaptive control technique, referred to as $\mathcal{L}_1$ adaptive control, which quickly compensates for large changes in the aircraft dynamics, providing an effective platform for aerobiological sampling.**

NOTATION

C_D	Drag force coefficient
C_T	Thrust coefficient
D	Drag force (N)
g	acceleration due to gravity (m/s^2)
I_{yy}	Pitch moment of inertia (kg m^2)
m	Mass (kg)
M	Pitch moment divided by pitch inertia I_{yy} (Nm/(kg m^2))
q	Pitch rate (deg/s)
S	Reference area (m^2)
T	Thrust (N)
V	Velocity (m/s)
Z	Vertical force divided by mass m (N/kg)
α	Angle of attack (deg)
δT	Thrust input
δe	Elevator deflection (deg)
θ	Pitch angle (deg)
ρ	Density of air (kg/m^3)

Dimensional stability derivatives are denoted by subscripts. For example, $M_\alpha = \frac{\partial M}{\partial \alpha}$. The same is the case for derivatives of dimensionless coefficients. For example, $C_{T_{\delta T}} = \frac{\partial C_T}{\partial \delta T}$.

I. INTRODUCTION

Plant pathologists and ecologists are naturally concerned with the dispersal, transport, and deposition of airborne biological particles, such as pollen or mold spores. Recent research, in which small UAVs were used to collect air samples in the planetary boundary layer (PBL), gives conclusive evidence that common plant pathogens can be transported over much greater distances than had previously been assumed [7]. Ref. [7] describes the use of remotely piloted UAVs, over a period of four years, to measure the relative abundance of viable spores of *Gibberella zeae*, the causal agent of Fusarium head blight in wheat. The UAVs were fitted with two spore-sampling devices, each consisting of two circular petri plates that are opened and closed like a clam shell while the UAV is in flight; see Figure 3. Each petri plate contained a Fusarium-selective medium which captured airborne spores for later cultivation in the laboratory. An example of an aerobiological culture is shown in the photograph in Figure 2. More recently, a similar sampling apparatus has been used to characterize the dispersal and transport of maize pollen in the surface boundary layer (SBL), as described in [1]. Advantages of using UAVs to collect such samples include extremely large sample volumes, which is important for collecting statistically significant samples of sparsely distributed particles, and a sampling method that is essentially independent of wind speed and direction [1].

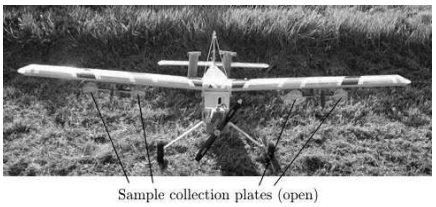

Fig. 1. A UAV with sample collection plates [7].

The use of a remotely piloted UAV for aerobiological sampling requires an experienced pilot and pilot availability may limit experimental research activities. Moreover, in applications where it is essential that the UAV maintain constant speed and altitude, a human pilot's performance may be inadequate. Autonomous flight control is an appealing alternative. For more ambitious experimental programs involving coordinated flight of multiple UAVs, automatic flight control is essential. Unfortunately, conventional automatic flight controllers do not adapt well to large changes in aircraft dynamics. In experiments involving a human pilot, sampling

This work was supported in part by ONR grant N00014-05-1-0516.

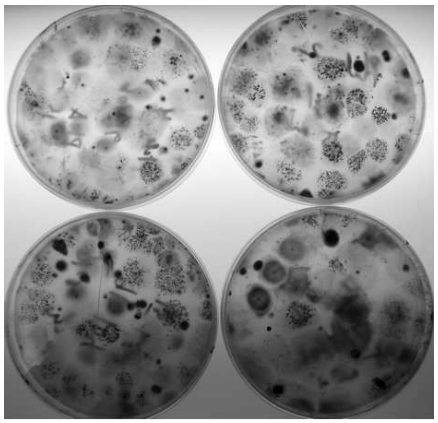

Fig. 2. Bacterial and fungal colonies cultured from samples collected within the PBL above Virginia Tech's Kentland Farm Microbial Observatory.

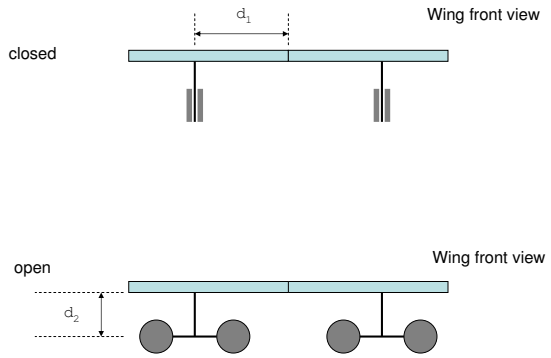

Fig. 3. Front view of the wing with dishes

plates such as those shown in Figure 3 are controlled by a second operator, allowing the pilot to concentrate entirely on recovering the aircraft from the large disturbance. Automatic flight control, for this application, would require a controller capable of rejecting large, fast disturbances. In this paper, we apply the newly developed $\mathcal{L}_1$ adaptive control method described in [2]–[4] to the problem of longitudinal control of a UAV used for aerobiological sampling. This robust control method provides fast adaptation and guaranteed transient performance in spite of large uncertainties in the system dynamics. Analysis and simulations for an aircraft of representative size illustrate the effectiveness of the approach.

II. Problem Formulation

We consider the special case of wings-level flight. Because the sampling plates are located symmetrically about the aircraft's symmetry plane, and because they open and close in unison, the three longitudinal degrees of freedom decouple from the remaining dynamics. Under reasonable assumptions, the airspeed dynamics are:

$$\dot{V} = \frac{1}{m}(T\cos\alpha - D) - g\sin\gamma.$$

If the angle of attack α and flight path angle γ remain small, this equation may be approximated as

$$\dot{V} = \frac{1}{m}(T - D) \tag{1}$$

where $T = \frac{\rho V^2}{2} S C_{T_{\delta T}} \delta T, \quad D = \frac{\rho V^2}{2} S C_D(\alpha)$. When the spore samplers open, as depicted in Figure 3, they generate an increment in drag and a nose-down pitch moment. Both disturbance effects are considered to be unknown functions of the angle of attack. The aerodynamic drag force becomes

$$D = \frac{\rho V^2}{2} S F(\alpha) \tag{2}$$

where the unknown nonlinear function $F(\alpha)$ represents the induced drag coefficient. The uncertainty in the drag force is largely due to the dramatic change in configuration associated with opening the spore samplers. The drag force certainly increases when the spore samplers are opened, but modelling this effect accurately, particularly while the plates are opening, is quite challenging. It is far more convenient to treat the effect as an uncertain disturbance.

In our control design step, we represent the uncertainty due to the increment in drag using step functions (i.e., we assume that the sampler plates open quickly). The magnitude of this step function is large and can easily compromise aircraft stability and performance. The control objectives, therefore, are to reject this disturbance by (1) modulating thrust in order to regulate the aircraft's speed and (2) modulating pitch control moment in order to regulate the aircraft's angle of attack.

Neglecting the influence of gravity and thrust on the angle of attack rate, and assuming the speed to be well-regulated by the thrust control loop, we consider the longitudinal dynamics to be well-described by equation (1) along with the following two equations:

$$\dot{\alpha} = \frac{1}{V_0}(Z_\alpha \alpha + Z_{\delta e}\delta e) + q \tag{3}$$

$$\dot{q} = M_\alpha \alpha + M_q q + M_{\delta e}\delta e \tag{4}$$

The first equation relates to the aircraft's vertical, or "plunge" dynamics while the second describes the pitch dynamics. We develop an "inner loop" controller for these dynamics with the understanding that a well-designed outer loop controller can then regulate the aircraft's altitude. Regarding equation (3), we will neglect the increment in total lift due to elevator deflections, as represented by the term $(Z_{\delta e}\delta e)/V_0$. This term is small compared to the other terms on the right hand side of equation (3). Note that we are working the "stability reference frame" so that, in nominal flight, the angle of attack and elevator deflection are zero.

Opening the sampling plates generates an incremental nose-down pitch moment:

$$\dot{q} = M_\alpha \alpha + M_q q + M_\delta \delta e - \Delta M \tag{5}$$

where $\Delta M > 0$. The sampling plate geometry and the parameters d_1 and d_2 shown in Figure 3 may be used to estimate the unknown force and moment, or at least to obtain bounds on the uncertainty.

Equations (1) and (3-4) may be written in the form

$$\dot{x}_1(t) = A_1 x_1(t) + B_1(u_1(t) + \Delta_1(x(t))) \quad (6)$$
$$\dot{x}_2(t) = A_2 x_2(t) + B_2(u_2(t) + \Delta_2(x(t))) \quad (7)$$

with the terms defined as follows:

$$\underbrace{[\dot{V}]}_{\dot{x}_1} = \underbrace{[0]}_{A_1}\underbrace{[V]}_{x_1} + \underbrace{[1]}_{B_1}[\underbrace{\frac{\rho V^2 S}{2m} C_{T_{\delta T}} \delta T}_{u_1} \underbrace{- \left(\frac{\rho V^2 S}{2m}\right)(C_D(\alpha)\eta_1(\alpha) + \eta_2(\alpha))]}_{\Delta_1}$$

$$\underbrace{\begin{bmatrix}\dot{\alpha}\\ \dot{q}\end{bmatrix}}_{\dot{x}_2} = \underbrace{\begin{bmatrix}\frac{Z_\alpha}{V_0} & 1\\ M_\alpha & M_q\end{bmatrix}}_{A_2}\underbrace{\begin{bmatrix}\alpha\\ q\end{bmatrix}}_{x_2} + \underbrace{\begin{bmatrix}0\\ M_{\delta e}\end{bmatrix}}_{B_2}[\underbrace{\delta e}_{u_2} \underbrace{- \frac{1}{M_{\delta e}}\Delta M}_{\Delta_2}].$$

It is reasonable to expect some conservative knowledge concerning the magnitude of the uncertainties Δ_i and their growth rates from analysis, experimental evaluation, or wind-tunnel testing. Thus, for $x_i(t) \in \mathcal{D}_i$, where $\mathcal{D}_i$ is some known compact set, we assume that the following uniform bounds hold with known positive constants L_i and D_i for $i \in \{1, 2\}$:

$$|\Delta_i(x_i') - \Delta_i(x_i'')| \leq L_i \|x_i' - x_i''\|$$
$$\max_{i=1,2} |\Delta_i(0)| \leq D_i$$

The two sets $\mathcal{D}_1$ and $\mathcal{D}_2$ will be specified shortly. The control objective is to maintain the nominal performance, i.e., to regulate the speed and altitude, in the face of these bounded uncertainties in drag force and pitch moment.

III. $\mathcal{L}_1$ Adaptive Control

Referring once again to equations (6) and (7):

$$\dot{x}_i(t) = A_i x_i(t) + B_i(u_i(t) - \Delta_i(x_i(t))), \quad x_i(0) = x_{i0} \quad (8)$$

where $i \in \{1, 2\}$. The controllers $u_i(t)$ are chosen for each subsystem in the following form:

$$u_i(t) = \underbrace{-K_i x_i(t)}_{u_{\mathrm{lin}_i}(t)} + u_{\mathrm{ad}_i}(t), \quad (9)$$

where $u_{\mathrm{lin}_i}(t)$ is the baseline linear controller for the i^{th} subsystem. These controllers may be designed using any standard linear control design technique. The control signal $u_{\mathrm{ad}_i}(t)$ is an adaptive element which augments the i^{th} baseline controller.

The subsystem uncertainties $\Delta_i(x_i)$ may be approximated to arbitrary precision within the compact set $\mathcal{D}_i$ using a linearly parametrized neural network. Specifically, we write

$$\Delta_i(x_i) = W_i^\top \Phi_i(x_i) + \epsilon_i(x_i), \quad x_i \in \mathcal{D}_i, \quad (10)$$

where $\Phi_i(x_i)$ is a vector of suitably chosen Gaussian basis functions of dimension $k_i \times 1$, $W_i \in \mathbb{R}^{k_i \times 1}$ is a vector of constant unknown parameters, and ϵ_i^* is a uniform bound for the approximation error over the set $\mathcal{D}_i$.

To derive the adaptive laws, consider the following predictor model:

$$\dot{\hat{x}}_i(t) = A_{m_i}\hat{x}_i(t) + B_i u_{\mathrm{ad}_i}(t) - B_i \hat{W}_i^\top(t)\Phi_i(x(t)), \quad \hat{x}_i(0) = x_{i_0}, \quad (11)$$

where $A_{m_i} = A_i - B_i K_i$ is a Hurwitz matrix. The predictor model leads to the following state error dynamics with $\tilde{x}_i(t) = \hat{x}_i(t) - x_i(t)$ and $\tilde{W}_i(t) = \hat{W}_i(t) - W_i$:

$$\dot{\tilde{x}}_i(t) = A_{m_i}\tilde{x}_i(t) - B_i \tilde{W}_i^\top(t)\Phi_i(x_i(t)) + B_i\epsilon_i(x_i), \quad \tilde{x}_i(0) = 0. \quad (12)$$

Since A_{m_i} is Hurwitz, by assumption, there exists a unique, positive definite solution P_i to the Lyapunov equation $P_i A_{m_i} + A_{m_i}^\top P_i = -Q_i$ for any symmetric positive definite matrix Q_i. Choose an adaptive gain $\Gamma_{i_c} > 0$ and define $\Gamma_i = \Gamma_{i_c}\mathbb{I}_k$ where $\mathbb{I}_k$ is the $k \times k$ identity matrix. Define the adaptation law

$$\dot{\hat{W}}_i(t) = \Gamma_i \mathrm{Proj}\left(\hat{W}_i(t), \Phi_i(x_i(t))\tilde{x}_i^\top(t)P_i B_i\right), \quad \hat{W}_i(0) = 0, \quad (13)$$

where $\mathrm{Proj}(\cdot,\cdot)$ represents the projection operator defined in [6]. This adaptation law ensures that all error signals remain bounded, regardless of the choice of $u_{\mathrm{ad}_i}(t)$. This does not ensure stability of the closed-loop system, however; one must define the adaptive control $u_{\mathrm{ad}_i}(t)$ and show that either $x_i(t)$ or, equivalently, $\hat{x}_i(t)$ is bounded. Moreover, one must define the set $\mathcal{D}_i$ and show that, with the given choice of adaptive control signal $u_{\mathrm{ad}_i}(t)$, the state $x_i(t)$ remains within $\mathcal{D}_i$ for all $t \geq 0$.

Consider the following $\mathcal{L}_1$ adaptive controller, given in the Laplace domain:

$$u_{\mathrm{ad}_i}(s) = C_i(s)\hat{r}_i(s), \quad (14)$$

where $C_i(s)$ is a low pass filter with unity DC gain and $\hat{r}_i(s)$ is the Laplace transform of $\hat{r}_i(t) \triangleq \hat{W}_i^\top(t)\Phi_i(x(t))$. To ensure stability of the entire system, one must show that the state of either (8) or (11) remains bounded with this choice of u_{ad_i}. The predictor model (11), with the control signal defined in (14), can be viewed as a linear time-invariant system with the input $\hat{r}_i(t)$. Let $\hat{x}_i(s)$ represent the Laplace transform of $\hat{x}_i(t)$. Then $\hat{x}_i(s) = \hat{G}_i(s)\hat{r}_i(s)$ where $\hat{G}_i(s) = H_{o_i}(s)(C_i(s) - 1)$ and $H_{o_i}(s) = (sI - A_{m_i})^{-1}B_i$. Note that $H_{o_i}(s)$ is a stable transfer function.

To ensure boundedness of the predictor system state and desired transient performance for the controller in (14), $C_i(s)$ must be selected such that

$$\|\hat{G}_i(s)\|_{\mathcal{L}_1} < \frac{1}{L_i}, \quad (15)$$

where $\|\cdot\|_{\mathcal{L}_1}$ denotes the $\mathcal{L}_1$ gain of $\hat{G}_i(s)$. In brief review, the $\mathcal{L}_1$-gain of a general system $H(s)$ is defined as:

$$\|H(s)\|_{\mathcal{L}_1} = \max_{i=1,..,n}\left(\sum_{j=1}^{m}\|H_{ij}(s)\|_{\mathcal{L}_1}\right),$$

in which $H_{ij}(s)$ is the i^{th} row j^{th} column element of $H(s)$ (for details refer to [2]–[4]). We further recall that the $\mathcal{L}_1$ gain of a stable proper single-input single-output system $H_{ij}(s)$ is defined as $\|H_{ij}(s)\|_{\mathcal{L}_1} = \int_0^\infty |h_{ij}(t)|dt$, where $h_{ij}(t)$ is the impulse response of $H_{ij}(s)$.

Following the approach in [2], let

$$\mathcal{D}_i = \{x \mid \|x\|_\infty \leq \gamma_{r_i} + \gamma_{1_i} + \gamma_{0_i} + \sigma_i\}, \qquad (16)$$

where $\sigma_i > 0$ is an arbitrary positive constant, while

$$\gamma_{r_i} = \frac{\|\hat{G}_i(s)\|_{\mathcal{L}_1}(D_i + \epsilon_i^*) + \|H_{o_i}(s)\|_{\mathcal{L}_1}\epsilon_i^*}{1 - \|\hat{G}_i(s)\|_{\mathcal{L}_1}L_i}, \qquad (17)$$

$$\gamma_{0_i} = \sqrt{\frac{\lambda_{\max}(P_i)}{\lambda_{\min}(P_i)}\left(\frac{2\epsilon_i^*\|P_iB_i\|}{\lambda_{\min}(Q_i)}\right)^2 + \frac{W_{\max_i}}{\lambda_{\min}(P_i)\Gamma_{c_i}}}, \qquad (18)$$

$$\gamma_{1_i} = \frac{(5\|\hat{G}_i(s)\|_{\mathcal{L}_1} + \|H_{o_i}(s)\|_{\mathcal{L}_1})\epsilon^*}{1 - \|\hat{G}_i(s)\|_{\mathcal{L}_1}L_i} + \frac{(1 + \|C_i(s) - 1\|_{\mathcal{L}_1})\gamma_{0_i}}{1 - \|\hat{G}_i(s)\|_{\mathcal{L}_1}L_i}, \qquad (19)$$

where $W_{\max_i} \triangleq 4 \max_{W_i \in \Theta_i} \|W_i\|^2$. The complete $\mathcal{L}_1$ adaptive controller consists of (8), (11), (13), and (14), all subject to condition (15) with $\mathcal{D}_i$ defined in (16).

IV. Analysis of the $\mathcal{L}_1$ Adaptive Controller

In this section we characterize the reference system, which is being tracked by the system (8) via the $\mathcal{L}_1$ adaptive controller both in transient and steady state. Following the approach in Refs. [2]–[4], consider the ideal version of the adaptive controller $u_{\mathrm{ad}_i}(t)$ in (14):

$$u_{\mathrm{ref}_i}(s) = \eta_i(s), \qquad (20)$$

where $\eta_i(s)$ is the filtered output of $W_i^\top \Phi_i(x_{\mathrm{ref}}(t))$ by $C_i(s)$. The closed-loop system with the ideal controller takes the form:

$$x_{\mathrm{ref}_i}(s) = \hat{G}_i(s)\eta_{1_i}(s) - H_{o_i}(s)\epsilon_i(s), \qquad (21)$$

where $x_{\mathrm{ref}_i}(s)$ is the Laplace transformation of the state $x_{\mathrm{ref}_i}(t)$ of the closed loop system, $\epsilon_i(s)$ and $\eta_{1_i}(s)$ are the Laplace transforms of the signals $\epsilon_i(x_{\mathrm{ref}}(t))$ and $W_i^\top \Phi_i(x_{\mathrm{ref}}(t))$, and $x_{\mathrm{ref}_i}(0) = x_{i_0}$. The following lemma states that the closed-loop system with the controller (20) is stable and its state remains inside $\mathcal{D}_i$ for all $t \geq 0$.

Lemma 1: [2] The control signal given by (20), subject to the condition in (15), ensures that the state of the closed-loop system in (21) remains inside $\mathcal{D}_i$ for all $t \geq 0$:

$$\|x_{\mathrm{ref}_i}\|_{\mathcal{L}_\infty} \leq \gamma_{r_i}. \qquad (22)$$

Thus, the control signal $u_{\mathrm{ref}_i}(s)$ ensures that for any $t \geq 0$ the state $x_{\mathrm{ref}_i}(t)$ remains inside the set $\mathcal{D}_i$, on which the neural network approximation has been defined. Next we need to show the uniform boundedness and the guaranteed transient performance of the $\mathcal{L}_1$ adaptive neural network controller. The main result from Ref. [2]–[4] is given by the following theorem.

Theorem 1: Given the system in (8), the reference system in (20), (21), and the $\mathcal{L}_1$ adaptive neural network controller defined via (11), (13), and (14) subject to (15), we have:

$$\|x_i - x_{\mathrm{ref}_i}\|_{\mathcal{L}_\infty} \leq \gamma_{1_i}, \qquad (23)$$

$$\|u_i - u_{\mathrm{ref}_i}\|_{\mathcal{L}_\infty} \leq \gamma_{2_i}, \qquad (24)$$

where γ_{1_i} is given in (19) and where

$$\gamma_{2_i} = \left\|C_i(s)(c_{o_i}^\top H_o(s))^{-1}c_{o_i}^\top\right\|_{\mathcal{L}_1}\gamma_{0_i} + \|C_i(s)\|_{\mathcal{L}_1}L_i\gamma_{1_i} + 3\|C_i(s)\|_{\mathcal{L}_1}\epsilon_i^*, \qquad (25)$$

with $c_{o_i} \in \mathbb{R}^n$ representing some vector for which $c_{o_i}^\top H_{o_i}(s)$ is minimum phase with relative degree one. (The existence of such a vector c_{o_i} is guaranteed; see [2].)

From the relationships in (22) and (23) it is straightforward to verify that $\|x_i\|_{\mathcal{L}_\infty} \leq \gamma_{r_i} + \gamma_{1_i}$ for any $t \geq 0$, i.e. $x_i(t) \in \mathcal{D}_i$.

Corollary 1: For the system in (8) and the $\mathcal{L}_1$ adaptive controller defined via (11), (13), and (14) subject to (15), we have:

$$\lim_{\Gamma_{c_i}\to\infty,\, \epsilon^*\to 0}(x_i(t) - x_{\mathrm{ref}_i}(t)) = 0, \quad \forall\, t \geq 0, \qquad (26)$$

$$\lim_{\Gamma_{c_i}\to\infty,\, \epsilon^*\to 0}(u_i(t) - u_{\mathrm{ref}_i}(t)) = 0, \quad \forall\, t \geq 0. \qquad (27)$$

Corollary 1 states that $x_i(t)$ and $u_i(t)$ follow $x_{\mathrm{ref}_i}(t)$ and $u_{\mathrm{ref}_i}(t)$ not only asymptotically but also during the transient, provided that the adaptive gain is selected sufficiently large and the neural network approximation is accurate enough. Thus, the control objective is reduced to selection of $C_i(s)$ to ensure that the reference system with unknown parameters has the desired response. In Ref. [3] and Ref. [4], specific design guidelines are provided for selection of $C_i(s)$ to achieve this objective. For the sake of brevity, we do not repeat those here. Nevertheless, the following remarks are in order [2]–[4].

Remark 1: If $C_i(s) = 1$, the $\mathcal{L}_1$ controller degenerates into a MRAC type. Then, the term $\left\|C_i(s)(c_{o_i}^\top H_{o_i}(s))^{-1}c_{o_i}^\top\right\|_{\mathcal{L}_1}$ in γ_{2_i} in (25) cannot be finite since $H_{o_i}(s)$ is strictly proper. Therefore, $\gamma_{2_i} \to \infty$, which implies that in conventional MRAC type neural network adaptive control, one can not reduce the bound of the control signal in (24) by increasing the adaptive gain or improving the approximation accuracy.

Remark 2: Recall that in the conventional MRAC scheme, the ultimate bound is given by γ_{0_i} defined in (18), which depends upon ϵ_i^*, $W_{\max_i}$ and Γ_{c_i}. While ϵ_i^* and $W_{\max_i}$ are related via the choice of radial basis functions (RBFs) used for approximation, Γ_{c_i} is a design parameter of the adaptive process that can be used to reduce the ultimate bound. However, increasing the adaptive gain in conventional MRAC leads to high-frequency oscillations in the control signal. With the $\mathcal{L}_1$ adaptive control architecture the ultimate bound of the tracking error is given by γ_{1_i} in (23). From the definition in (19), it follows that $\gamma_{1_i} > \gamma_{0_i}$. Nevertheless, the ability of the $\mathcal{L}_1$ adaptive control architecture to tolerate high adaptive gains implies that γ_{0_i} can be reduced leading to an overall smaller value for γ_{1_i}. This ability is enabled via the low-pass system in the feedback path that filters out the high-frequencies in $\hat{W}_i(t)^\top \Phi_i(x(t))$ excited by large Γ_{c_i}.

Fig. 4. The Sig Rascal 110.

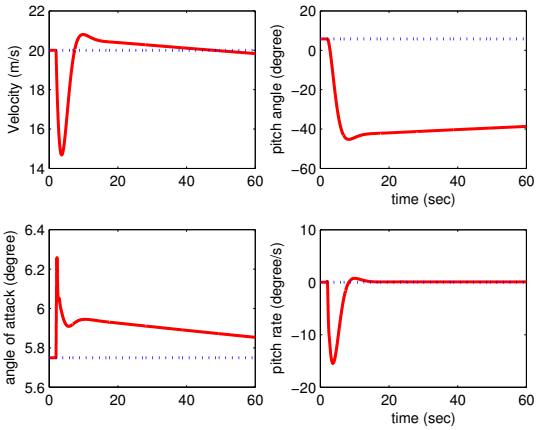

Fig. 5. State Trajectories without $\mathcal{L}_1$ control: velocity, α, θ and altitude (solid line: with uncertainties; dotted line: nominal)

V. Simulation Results

A simulation example is presented to illustrate the benefit of the $\mathcal{L}_1$ adaptive controller. The aircraft model parameters used in the simulation correspond to the Sig Rascal 110, the airframe which is used for UAV control research in Virginia Tech's Nonlinear System Laboratory [5]. The aircraft starts from trim conditions $\alpha = 5.75$ deg, $\theta = 5.75$ deg, and $V_0 = 20$ m/s. After 2 seconds, the petri plates are opened, resulting in a sudden change in the drag force and the pitching moment.

In nominal conditions, with the petri plates closed, the linear control law provides adequate regulation of the trim state. Figure 5 shows the state history once the petri plates are open. From the figures it can be seen that the velocity, pitch angle and angle of attack all deviate significantly from their nominal values; the airplane begins diving.

Next, we apply the $\mathcal{L}_1$ adaptive controller to this scenario. First, we examine the growth rate of the assumed uncertainties and compare their inverse to the $\mathcal{L}_1$ gains of $\hat{G}_i(s)$ in order to choose the bandwidths ω_i of the low pass filters $C_i(s)$. The transfer function $\hat{G}_i(s)$ represents a cascaded system of low pass filter $H_{o_i}(s)$ and high pass filter $(C_i(s) - 1)$. Thus $\|\hat{G}_i(s)\|_{\mathcal{L}_1}$ can be reduced when

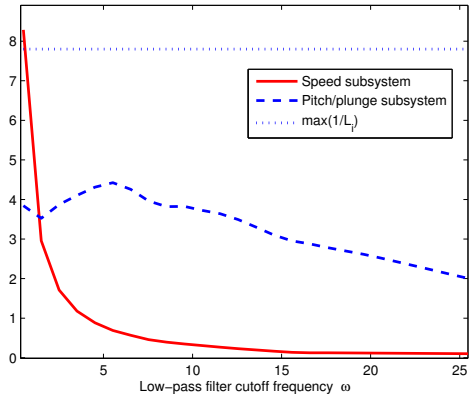

Fig. 6. Comparison of $\|\hat{G}_i(s)\|_{\mathcal{L}_1}$ and $1/L_i$; see inequality (15).

the bandwidth of the low pass filter $C_i(s)$ is increased. It is safe enough to compare the inverse of the largest possible growth rate of the uncertainties to $\|\hat{G}_i(s)\|_{\mathcal{L}_1}$. We calculate the $\mathcal{L}_1$ gains of $\hat{G}_i(s)$ at different values of bandwidth ω numerically, and choose a large enough bandwidth to satisfy the $\mathcal{L}_1$ gain stability requirement. Based on the chosen uncertainties, we select the larger (conservative) growth rate as $L_{\max} = \max\{L_1, L_2\} = 0.1270$. Figure 6 indicates a lower bound on the choice of the filter's cutoff frequency. Choices which satisfy this bound and provide good performance are $\omega_1 = 10$ and $\omega_2 = 5$.

As shown in Figure 7, when the system is subjected to the same large disturbance with an $\mathcal{L}_1$ adaptive controller implemented, the nominal performance is recovered. The adaptive gains of for the $\mathcal{L}_1$ controller were chosen quite high, $\Gamma = 5000\mathbb{I}$, in order to achieve fast adaptation. The control signal, however, exhibits only low frequency components due to the low pass filters. When the uncertainties change, there is no need to re-tune the adaptive gain, while in conventional MRAC re-tuning may be needed. The next example, illustrated in Figure 8 shows that when the amplitude of the uncertainties increase by two times, the same $\mathcal{L}_1$ controller still recovers the nominal performance without additional tuning.

Figure 9 shows the control inputs (elevator and throttle inputs) using the $\mathcal{L}_1$ adaptive controller for two different values of uncertainties. The control signals are low frequency signals even with very large adaptive gains. For different values of the uncertainties, the control signals show scaled responses, which is characteristic of a linear system. One of the benefits of $\mathcal{L}_1$ adaptive control is that it guarantees the system's control signals track those of a linear reference system within bounds stipulated by designers, both during the transient and at steady state.

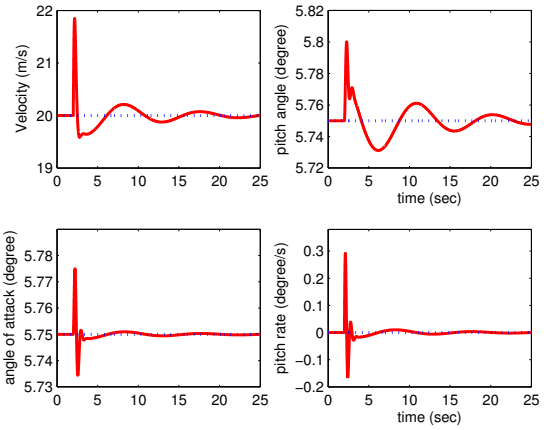

Fig. 7. State histories using $\mathcal{L}_1$ adaptive control: V, α, θ and q. (Solid line: with uncertainties; dotted line: nominal)

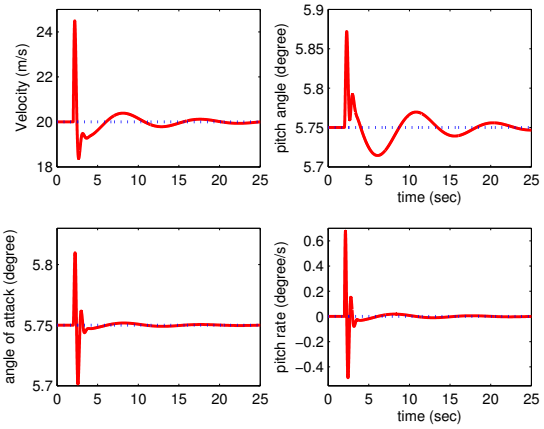

Fig. 8. State histories with $\mathcal{L}_1$ adaptive control for larger uncertainties: V, α, θ and q. (Solid line: with uncertainties; dotted line: nominal)

VI. Conclusion

This paper describes a well-motivated application of the newly developed $\mathcal{L}_1$ adaptive control theory to flight control of small UAVs for aerobiological sampling. Because the sampling mechanisms for these UAVs introduce sudden, dramatic changes in flight characteristics, It is necessary for an autopilot to adapt quickly and with guaranteed robustness and transient performance. Simulations illustrate the control designer's ability to choose large adaptation gains for fast convergence without compromising robustness. Simulations illustrates the fact that the adaptive controller does not require re-tuning of the adaptive gains for different reference signals. These observations are consistent with the rigorous theory that underlies the method, as described in the references. It is expected that well-regulated autonomous UAVs equipped with aerobiological sampling devices will soon provide enormous insight into atmospheric microbial communities and their relationship to agricultural ecosystems.

VII. Acknowledgement

The authors gratefully acknowledge Dr. Chengyu Cao for his thoughtful comments and contributions to this work.

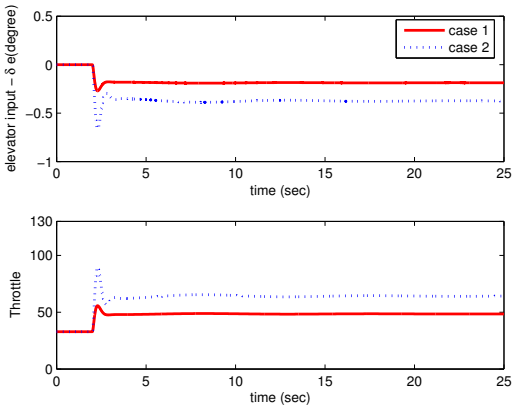

Fig. 9. Control effort using $\mathcal{L}_1$ adaptive control with two uncertainty values.

References

[1] D. E. Aylor, M. T. Boehm and E. J. Shields, Quantifying aerial concentrations of maize pollen in the atmospheric surface layer using remote-piloted airplanes and Lagrangian stochastic modeling, *Journal of Applied Meteorology and Climatology*, pages 1003-1015, Vol. 45, July 2006.

[2] C. Cao and N. Hovakimyan, Novel $\mathcal{L}_1$ neural network adaptive control architecture with guaranteed transient performance, Accepted for publication in invited issue of *Invited issue of IEEE Transactions on Neural Networks on Feedback Control*, 2006.

[3] C. Cao and N. Hovakimyan, Design and analysis of a novel $\mathcal{L}_1$ adaptive controller, Part I: Control signal and asymptotic stability, *American Control Conference*, pages 3397-3402, 2006.

[4] C. Cao and N. Hovakimyan, Design and analysis of a novel $\mathcal{L}_1$ adaptive controller, Part II: Guaranteed transient performance, *American Control Conference*, pages 3403-3408, 2006.

[5] L. Ma, V. Stepanyan, C. Cao, I. Faruque, C. Woolsey, and N. Hovakimyan, Flight test bed for visual tracking of small UAVs, *AIAA Guidance, Navigation, and Control Conference and Exhibit*, Keystone, CO, Aug. 21-24, AIAA-2006-6609.

[6] J. Pomet and L. Praly, Adaptive nonlinear regulation: Estimation from the Lyapunov equation, *IEEE Transactions on Automatic Control*, 37(6):729-740, 1992.

[7] S. L. Maldonado-Ramirez, D. G. Schmale III, E. J. Shields and G. C. Bergstrom, The relative abundance of viable spores of *Gibberella zeae* in the planetary boundary layer suggests the role of long-distance transport in regional epidemics of Fusarium head blight, *Agricultural and Forest Meteorology*, pages 20-27, Vol. 132, 2005.